Editors' Suggestion

Unidirectional Chiral Magnonics in Cylindrical Synthetic Antiferromagnets

R.A. Gallardo,[1,*] P. Alvarado-Seguel,[2] and P. Landeros[1,†]

[1] *Departamento de Física, Universidad Técnica Federico Santa María, Avenida España 1680, Valparaíso, Chile*
[2] *Departamento de Matemáticas, Universidad de Chile, Las Palmeras 3425, Ñuñoa, Santiago, Chile*

(Received 2 June 2022; revised 4 August 2022; accepted 28 September 2022; published 15 November 2022)

Asymmetric spin-wave propagation in magnetic nanostructures has received significant attention due to the potential applications of magnon-based devices. In curved nanostructures and planar multilayers, the classical dipole-dipole interaction induces a significant frequency nonreciprocity in which two counterpropagating waves excited at the same frequency exhibit different wavelengths. This work proposes a cylindrical synthetic antiferromagnet as a potential three-dimensional waveguide design to generate nonreciprocal spin waves. The magnetochiral properties emerge from two mechanisms: the asymmetric interlayer dipolar coupling and the asymmetric dipolar coupling of the curved membrane. It is demonstrated that the cylindrical bilayer presents a notable spin-wave asymmetry induced by the combined action of antiparallel magnetic vortices and the curvature of the inner and outer surfaces. A substantial frequency range with waves having only a negative phase velocity is predicted, where unidirectional wave propagation is allowed. It is also found that the nonreciprocity reaches a constant value as the curvature decreases, which is an essential advantage over isolated nanotubes, where the frequency shift vanishes at a large radius. Besides, analytical expressions are proposed to predict the frequency shift in the case of coupled cylindrical shells. These results are relevant from fundamental and practical points of view since magnetochirality is a crucial ingredient in visualizing future spin-wave-based logic devices.

DOI: 10.1103/PhysRevApplied.18.054044

I. INTRODUCTION

Spin waves (SWs) are collective excitations in magnetic systems and the essential physical element in the area of magnonics [1–6]. The diverse ways of manipulating the spin-wave band structure represent the main attraction for the scientific community focused on magnonics, which utilizes propagating waves for nanoscale transmission and information processing [7]. In terms of applications, the collective nature of the SWs implicates low energy dissipation in the chargeless transport of information since there is a reduced Joule heating. Therefore, SWs present a clear advantage over diffusive transport in electronics, where the charge motion results in collisions that become more prominent in densely packed elements [1,3]. Another exciting feature is that the magnon wavelengths are orders of magnitude shorter than those of electromagnetic waves at the same frequency [8–11], which facilitates the miniaturization of technological devices [12,13]. Moreover, the possibility of preparing different magnetic phases allows for the easy reconfigurability of the band structure, which relies on the internal magnetic field landscape [14,15].

One of the best technical attributes of spin waves is their strongly anisotropic dispersion, which can be tailored by design and external control, allowing for the propagation of information through a hierarchy of bulk and surface waves [16]. Under certain conditions, some spin-wave modes may behave nonreciprocally, where two opposing waves display different wavelengths at the same frequency [7]. More dramatically, SW propagation may be forbidden in some orientations, allowing one to build magnonic diodes [17]. Several applications based on nonreciprocal SWs have been proposed, such as magnonic circulators, isolators, phase shifters, and logic devices [18–21].

Different types of magnetic systems are characterized for presenting a nonreciprocal SW propagation, for instance, magnetization-graded films [22], magnetic nanotubes [23–29], curvilinear magnetic shells [25], arrays of nanopillars [30], coupled ferromagnetic bilayers [31–41], heavy-metal/ferromagnetic bilayers [42–51], noncentrosymmetric chiral magnets [52–56], and some types of magnonic crystals [57–59]. In the case of synthetic antiferromagnets (SAs), a strong nonreciprocity has been reported, where the dynamic dipolar interaction is its physical source [36,37], and its magnitude is notably enhanced as the thicknesses of the magnetic layers increase [40]. Interestingly, for an antiparallel alignment of ferromagnetic layers, the dynamical dipolar energy

*rodolfo.gallardo@usm.cl
†pedro.landeros@usm.cl

is reduced only for one propagation direction, wherein the stray fields and dynamic magnetizations form a flux-closure dynamical state [36]. Reconfigurability of the spin-wave spectrum is also expected in SAs since the antiparallel magnetization state, where the nonreciprocity is active, can be switched to a parallel state just by increasing the field [36]. Topological properties have also been calculated in antiparallel-aligned magnetic multilayers, where the chiral dipolar interaction between propagating magnons generates bulk bands with nonzero Chern integers [60]. SW asymmetry induced by dipolar interaction has even been obtained in parallel-coupled bilayers as long as they have different thicknesses or magnetic parameters [41].

Under specific conditions, the nonreciprocity in the dispersion can also lead to the surprising phenomenon of *unidirectional* magnon propagation [61]. Such behavior has been reported for Damon-Eshbach SWs in magnetic films [62] based on the well-known amplitude nonreciprocity of magnetostatic surface waves [16,63]. Micromagnetic simulations revealed a unidirectional SW transmission in magnonic waveguides with interfacial Dzyaloshinskii-Moriya interaction [64,65]. Unidirectional spin-wave channeling along Bloch-type magnetic domain walls has been further reported, which relies on the stability of the magnetic texture [66]. Chen *et al.* reported the unidirectional conduction of SWs in an ultrathin Yttrium iron garnet (YIG) film capped with an array of Co wires [67]. The phenomenon of resilience to back reflection by boundaries or defects has been demonstrated in SAs, which naturally arises from the combination of low anisotropy and nonreciprocity [39]. Based on dipolar nonreciprocity, a spin-wave diode has been proposed in a Co-Fe-B/Py SA, where the low group velocities along one direction allow for unidirectional propagation [41]. The coupled magnonic modes in a system with two ferromagnetic layers, with one covered with heavy metal, were also proposed for the realization of SW diodes and circulators [68]. Nevertheless, the unidirectional SW propagation in most of these nanostructures is based on amplitude nonreciprocity, which means that SWs will transmit in both directions but with a smaller amplitude in one of them. Therefore, it is highly desirable to design magnonic nanostructures that permit unidirectional SW steering with prohibited states in a broad range of wave vectors and frequencies.

Three-dimensional magnetic nanostructures have been investigated extensively in the last few decades, evidencing novel magnetic phases and reversal mechanisms [69–75]. In the thin nanotube case, the propagation of a vortex domain wall depends on the initial chirality of the wall due to the asymmetry of the demagnetizing field [76–78]. Such magnetochiral effects have been reported in curved nanostructures [79–83], where, in the case of circular nanotubes, the physical origin is the dipolar interaction and the curvature-induced geometrical charge [25,76]. A notable SW asymmetry has been theoretically reported in thin ferromagnetic nanotubes (NTs) when the spin waves propagate along the tube while the equilibrium magnetization is in a vortex state [23–29]. It has been further predicted that SW nonreciprocity is present in the zeroth-order and higher-order azimuthal modes and increases with the NT thickness [28,29]. Recent measurements with time-resolved scanning transmission x-ray microscopy evidenced the nonreciprocal dispersion of hexagonal nanotubes, where localized modes were observed in the highly curved corners and flat edges [84]. The degenerate nature of the modes with azimuthal wave vectors known from round tubes is partly lifted in hexagonal nanotubes, resulting in singlet and duplet modes [84]. A characteristic of curvature-induced symmetry breaking is that, for increasing radii, the frequency shift (frequency difference of two counterpropagating waves evaluated at a fixed wave-vector magnitude) decreases because of the negligible influence of curvature. Namely, as the curvature decreases, the nanotube tends to a planar membrane, where the frequency nonreciprocity vanishes [28].

This paper proposes a cylindrical synthetic antiferromagnet (CSA) as a nonreciprocal and unidirectional magnonic waveguide. The nanostructure comprises two antiparallel coupled nanotubes, where a vortex ground state is established in each nanotube. The dynamic matrix method is utilized to calculate the temporal evolution of the magnetization so that the system is not limited to thin tubes [28]. There is a wide range of frequencies in the CSA design, where spin waves have only negative phase velocity, which leads to diodelike propagation. There are two contributions to the dipolar field that behave as chirality sources. The first is the asymmetric field from interlayer dipolar coupling [36] and the second is the contribution of curvature [23]. The combined influence of the two mechanisms is studied, where it is found that the proposed architecture preserves the dynamic chiral properties as the curvature of the NT is reduced, which is a remarkable difference concerning an isolated NT, where the SW asymmetry tends to zero as the curvature decreases. It is also demonstrated that both planar and cylindrical synthetic antiferromagnets have similar dynamic properties when the layers are thin. An analytical formula is presented to understand the nonreciprocal properties of the cylindrical synthetic antiferromagnets.

II. THEORETICAL METHOD

The model follows Ref. [28], where an in-house-developed theory based on the dynamic matrix method [85,86] is used. The method goes beyond the ultrathin approach and allows for the description of thick nanotubes, where the usually ignored radial inhomogeneity of the dynamic magnetization is taken into account. The increment in the thickness d is essential to enhance the

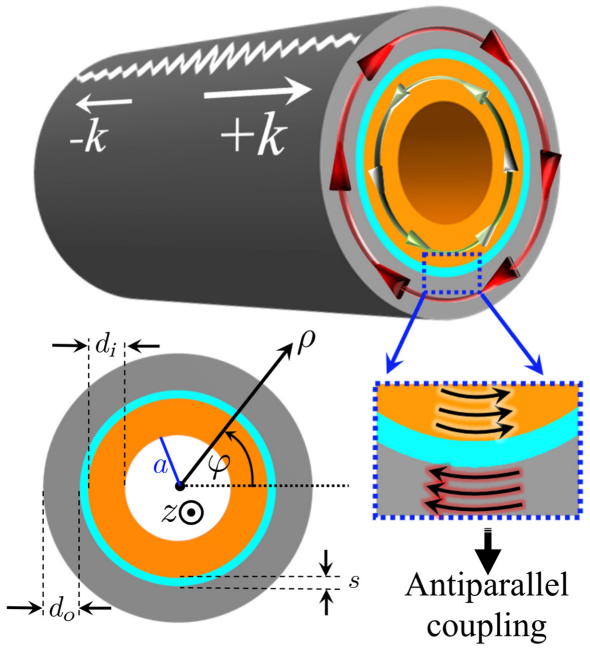

FIG. 1. A cylindrical synthetic antiferromagnet is illustrated. The spin waves propagate along the symmetry axis, where a vortex equilibrium configuration is assumed for both nanotubes. The inner tube has a counterclockwise orientation, while the outer one presents a clockwise vortex state. The thickness of each nanotube is denoted by d_i and d_o, which correspond to the inner and outer nanotubes, respectively. The nonmagnetic shell that separates the magnetic NTs has a thickness s, while the inner radius of the system is a. The insets depict the notation and the antiparallel vortices.

dipolar nonreciprocity that scales with d [36], instead of the chiral behavior established with interfacial Dzyaloshinskii–Moriya interaction (DMI), which scales with $1/d$ [45] and undesirably enlarges damping [87] while decreasing the spin-wave lifetime. The theory is applied to the case of a cylindrical synthetic antiferromagnet, where two coaxial tubes are coupled. An interlayer exchange interaction of the type $\epsilon_{\rm ex} = -\xi(\mathbf{M}^n \cdot \mathbf{M}^p)/(M_s^2)$ is used to stabilize the antiparallel configuration (see Fig. 1). Here, M_s is the saturation magnetization, ξ is an interlayer exchange constant with energy/length units, and n,p refers to the ferromagnetic cylindrical layer at the nonmagnetic/ferromagnetic interface. To account for the left- and right-handed orientations of the vortex, the equilibrium magnetizations are written as $\mathbf{M}^n_{\rm eq}(\mathbf{r},t) = C_n M_s^n \hat{\boldsymbol{\varphi}}$. Here, the factor C_n describes the chirality of the vortex magnetization at each layer; in the case of counterclockwise orientation $C_n = 1$, while for the clockwise case $C_n = -1$. In what follows, the local basis $(\hat{\mathbf{e}}_1^n, \hat{\mathbf{e}}_2^n, \hat{\mathbf{e}}_3^n) = (\hat{\boldsymbol{\rho}}, C_n\hat{\boldsymbol{\varphi}}, C_n\hat{\mathbf{z}})$ induced by the chirality of each layer is used. It is noted that the relation of the dynamic magnetization components in both bases is $(m_\rho^n, m_\varphi^n, m_z^n) = (m_1^n, C_n m_2^n, C_n m_3^n)$.

From $\epsilon_{\rm ex}$, the components of the exchange interlayer effective field acting in the cylindrical shell n are:

$$(h^n_{\rm inter})_1 = \sum_{<p>} \frac{J^{np}_{\rm ex}}{M_s^2 S(n)} m_1^p, \tag{1}$$

$$(H^n_{\rm inter})_2 = \sum_{<p>} \frac{J^{np}_{\rm ex}}{M_s^2 S(n)} C_n C_p, \tag{2}$$

$$(h^n_{\rm inter})_3 = \sum_{<p>} \frac{J^{np}_{\rm ex}}{M_s^2 S(n)} C_n C_p m_3^p, \tag{3}$$

where the sum is over neighboring layers. In the case of a cylindrical synthetic antiferromagnet, $J^{np}_{\rm ex} < 0$ at the interface, that is, whenever $C_n = -C_p$. On the other hand, by keeping in mind that both NTs are divided into many sublayers, the dipolar interaction between cylindrical shells can be accounted for by following Ref. [28], where the dynamic effective dipolar fields are written as $\mathbf{h}^n = -\sum_p \Lambda^{np}_{\rm dip} \cdot \mathbf{m}^p$. Then, the dynamic demagnetizing tensor $\Lambda^{np}_{\rm dip}$, with respect to the local basis, is given by

$$(\Lambda^{np}_{\rm dip})_{11} = \iiint \rho' \partial_{\rho\rho'} G(\rho,\rho',\varphi') d\rho d\rho' d\varphi', \tag{4a}$$

$$(\Lambda^{np}_{\rm dip})_{31} = ikC_n \iiint \rho' \partial_{\rho'} G(\rho,\rho',\varphi') d\rho d\rho' d\varphi', \tag{4b}$$

$$(\Lambda^{np}_{\rm dip})_{13} = -ikC_p \iiint \rho' \partial_{\rho} G(\rho,\rho',\varphi') d\rho d\rho' d\varphi', \tag{4c}$$

$$(\Lambda^{np}_{\rm dip})_{33} = k^2 C_n C_p \iiint \rho' G(\rho,\rho',\varphi') d\rho d\rho' d\varphi'. \tag{4d}$$

Here, k represents the z component of the wave vector and function $G(\rho,\rho',\varphi')$ is defined in Eq. (11) of Ref. [28]. The uniaxial anisotropy contribution can also be found in Ref. [28], while the external field is assumed to be zero.

III. RESULTS AND DISCUSSION

For the calculations, permalloy (Py: $Ni_{80}Fe_{20}$) magnetic parameters are chosen for both tubular layers, where the saturation magnetization and the exchange constant are $M_s = 796$ kA/m and $A_{\rm ex} = 13$ pJ/m, respectively. A uniaxial anisotropy is used to stabilize the equilibrium vortex state of the magnetization for each tube, where the anisotropy constant is $K_u = -50$ kJ/m^3 [26], which compensates for the exchange interaction arising in the vortex state. Note that the negative value of K_u implies that an orientation perpendicular to the z axis is favored, stabilizing both the clockwise and counterclockwise vortices. The magnitude of the gyromagnetic ratio is $\gamma = 175.929$ GHz/T, while the exchange constant is $\xi = -160\pi \times 10^{-9}$ mJ/m [88]. The magnetization must be free to change along with the NT thickness. Therefore, according to the dynamic matrix method, the thick

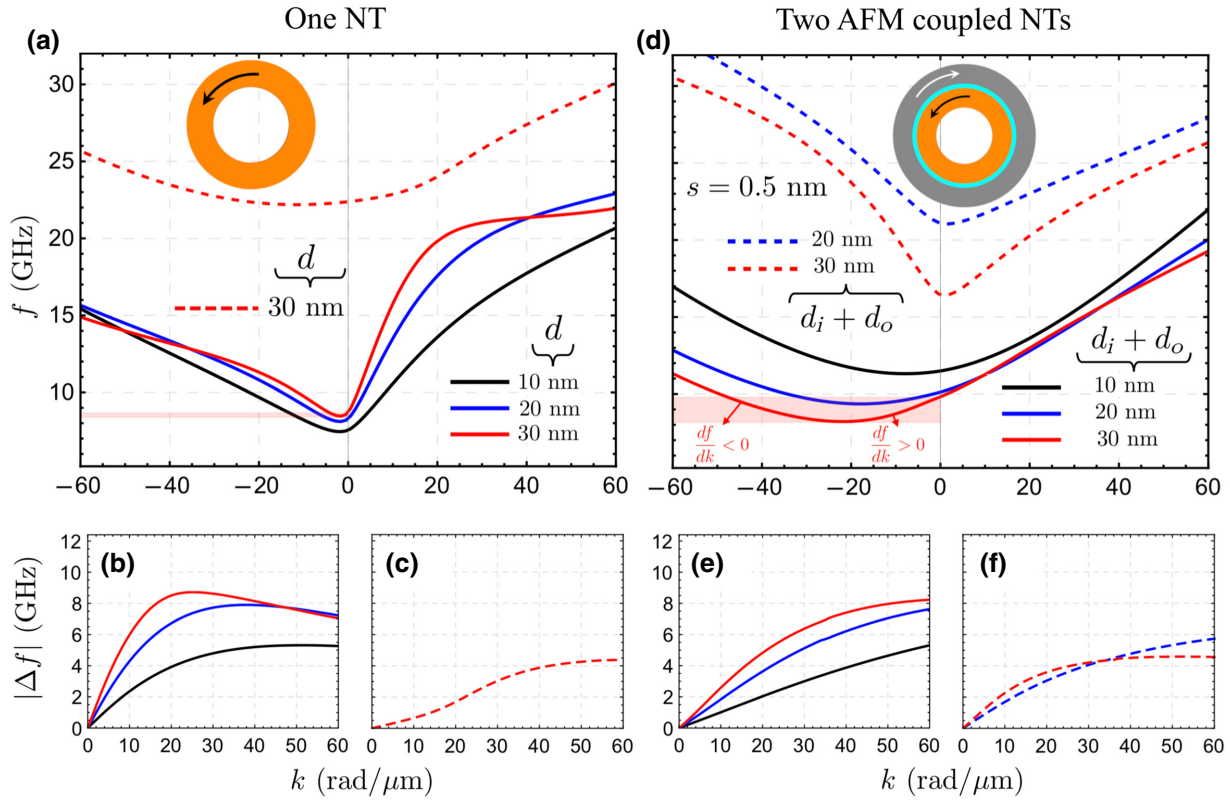

FIG. 2. Spin-wave dispersion and frequency shift for single and bilayer nanotubes with internal radius $a = 20$ nm. (a)–(c) An isolated nanotube is considered. (d)–(f) The curves are calculated for the proposed cylindrical synthetic antiferromagnet. In the case of one NT, calculations are realized for thicknesses of 10 nm (black), 20 nm (blue), and 30 nm (red). In the bilayer nanotube, the thickness of both layers is $d_i + d_o = 10$ nm, 20 nm, and 30 nm (with $d_i = d_o$). The thickness of the spacer is $s = 0.5$ nm. In (a),(d), the solid lines correspond to the zeroth-order modes, while the dashed lines to the first-order modes. The bottom panels represent the frequency shift versus the wave vector for the different modes. The red shaded zone depicts the frequency and wave-vector range, for the case $d_i + d_o = 30$ nm, where the group velocity is positive and negative, while the phase velocity is negative.

nanotube is divided into thinner cylindrical layers (of 1 nm in thickness), coupled through dipolar and exchange interactions.

Figure 2 shows the SW dispersion of an isolated nanotube [Fig. 2(a)] and a cylindrical synthetic antiferromagnet [Fig. 2(d)]. The thickness of the isolated NT is d, while the thickness of the CSA is d_i (d_o) for the inner (outer) tube. Exemplary tubular shells of $d = 10, 20$, and 30 nm are considered in Fig. 2(a), while $d_i + d_o = 10, 20$, and 30 nm (with $d_i = d_o$) in Fig. 2(d). The spacer thickness is $s = 0.5$ nm, and the internal radius is $a = 20$ nm. The results show that both systems present dynamic chiral features due to the dipolar interaction, evidenced by the asymmetric spin-wave dispersion. Such an asymmetry increases with the shell thicknesses, where standing radial waves are observed at affordable frequencies when d is large [see dashed line in Fig. 2(a)]. In the case of a cylindrical synthetic antiferromagnet, two SW modes are observed for $d_i = d_o = 20$ and 30 nm, while only the lowest SW branch is observed for $d_i = d_o = 10$ nm. Higher-order modes are also excited in both isolated and coupled tubular systems, but at frequencies higher than 32 GHz. Note that the SW dispersion of the high-frequency modes shown in Fig. 2(d) has larger frequencies for the negative wave vectors, while the opposite is obtained for the low-frequency branches. This behavior can be explained by analyzing the theory described in Ref. [36] for a planar SA, where one can show that for the lowest SW branch, a flux-closure dynamical state is obtained at negative wave vectors, which implies a reduction of the dynamic dipolar energy is reached for such negative wave vectors (see Fig. 3 of Ref. [36]). Then, similar behavior is obtained for the high-frequency mode, but in this case, the flux-closure dynamical state is given at positive wave vectors. Such asymmetry can also be seen from Eqs. (1) and (2) in Ref. [36], where there is a clear difference in sign between the first and second mode, especially in the first term of each equation. Figures 2(b), 2(c), 2(e), and 2(f) depict the magnitude of the frequency shift as a function of the wave vector $\mathbf{k}$. Such a frequency shift is defined as $\Delta f = f(\mathbf{k}) - f(-\mathbf{k})$. Here, it is observed that the maximum value of $|\Delta f|$ is similar in both systems, while such a quantity is given at different wave vectors (see

lower panels in Fig. 2). As the internal radius increases, the frequency shift of the isolated tube decreases, while a completely different behavior occurs for the cylindrical synthetic antiferromagnet, which is discussed below. An attractive characteristic of the magnonic dispersion of the bilayer nanotube is that it manifests a broad range of frequencies where the phase velocity is negative, while the group velocity can be positive ($df/dk > 0$) or negative ($df/dk < 0$). In the red shaded zones shown in Figs. 2(a) and 2(d), one can observe that, in the case of a thickness of 30 nm, the frequency range increases from approximately 0.3 GHz for a single NT to 2 GHz for two coupled NTs. This behavior can be helpful since it allows inducing resilience to back reflections caused by defects [39], which makes the SW propagation more robust.

The SW dispersion of the low-frequency mode is further explored as a function of the anisotropy and the shell thicknesses. Figure 3(a) shows the dispersion of two thick coaxial shells of the same thickness ($d_i = d_o = 25$ nm) for different ratios of the uniaxial anisotropy, where the reference anisotropy constant is $K_u = -50$ mJ/m^3. One can observe that, at zero fields, the minimum of the lowest SW branch approaches the $k = 0$ state as $|K_u^i| < |K_u^o|$. Of course, for this analysis, at least one of the anisotropies is finite to make the vortex equilibrium configuration stable. If both anisotropies decrease in magnitude, the minimum of the SW dispersion reaches the zero frequency point, where the vortex equilibrium becomes unstable. In the presence of an external field, the dispersion moves up without altering the minimum wave-vector position (not shown). Another interesting behavior occurs when both cylindrical shells have different thicknesses. In Fig. 3(b), only the cases $d_i = 5$ nm and $d_o = 45$ nm; and $d_i = 15$ nm and $d_o = 35$ nm have different thicknesses. If the thicknesses are not too different (case $d_i = 15$ nm and $d_o = 35$ nm), the SW dispersion is not notably modified. Nonetheless, if the thickness asymmetry is more pronounced (see case $d_i = 5$ nm and $d_o = 45$ nm), the mode excited in one direction is characterized by having a low group velocity in a broad wave-vector range [see the shaded area in Fig. 3(b)]. This behavior is understood by considering the dispersion of one NT. The dashed black line in Fig. 3(b) shows the case of one NT with $d = 45$ nm, where the group velocity is negative at $k < 0$ after a frequency minimum close to $k = 0$ (see inset). In contrast, for two coupled NTs with the same thickness [see solid blue line in Fig. 3(b) for $d_i = d_o = 25$ nm], the group velocity is positive at $k > -20$ rad/μm. Thus, as the thickness of one of the NTs decreases, the cylindrical bilayer's dispersion approaches that of an isolated nanotube. Thus, there is a transition from $df/dk < 0$ to $df/dk > 0$. This transition implies that at a given point, the group velocity must be close to zero, which is observed in Fig. 3(b) (see open triangles). One can also see that the minimum of the SW dispersion close to $k = 0$ (for one NT) is also present in the

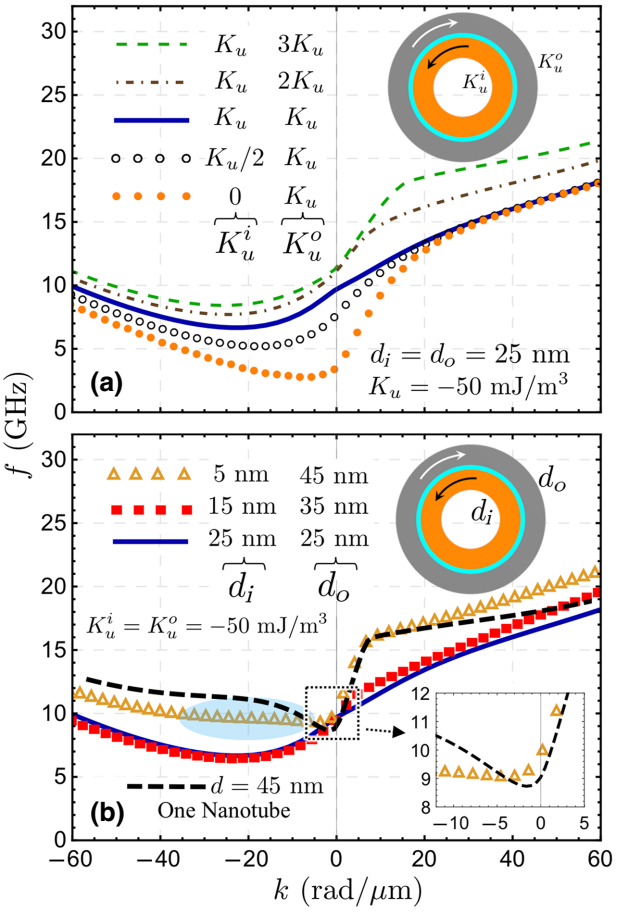

FIG. 3. SW dispersion of the low-frequency mode of a bilayer nanotube for varying anisotropies and thicknesses. (a) Cases with different anisotropies are analyzed, where the reference value is $K_u = -50$ mJ/m^3. The anisotropy of the inner (outer) nanotube is described by K_u^i (K_u^o), and the thickness of each layer is 25 nm. (b) The total thickness of the system is kept fixed, while the thicknesses in both layers are varied. d_i and d_o correspond to the thickness of the inner and outer nanotubes, respectively. The shaded zone in (b) highlights the range of frequencies and wave vectors with a small magnitude of the group velocity, while the inset shows the dispersion of one NT (with $d = 45$ nm) and the case of a CSA with $d_i = 5$ nm and $d_o = 45$ nm. All calculations are realized for $a = 20$ nm.

case $d_i = 5$ nm and $d_o = 45$ nm of the cylindrical synthetic antiferromagnet [see inset in Fig. 3(b)].

The curvature-induced symmetry breaking caused by the dipolar interaction can be attributed to two processes: first, the geometrical charges induced by the curvature [25]; and second, the flux-closure dynamical state induced by the antiferromagnetic alignment of the magnetizations. The latter is present in a planar synthetic antiferromagnet, where the geometrical charges are absent [36,39,41]. In Fig. 4(a), the frequency shift (evaluated at $|k| = 20$ rad/μm) is calculated as a function of the internal radius, where the curvature effects decay with a. The single

nanotube case shows the expected behavior with increasing radius (open circles), where nonreciprocity decays as $1/a$; an inner radius considerably more significant than the exchange length has vanishing magnetochiral effects from curvature [28]. Interestingly, this is not the case for a tubular magnetic bilayer, where the frequency shift (filled circles) converges to a constant value as the curvature radius increases. Indeed, as shown by the dashed line in Fig. 4(a), such a value approximates that of a planar synthetic antiferromagnet [89]. The SW dispersions of the synthetic antiferromagnets (planar and tubular) are also similar as the curvature decreases. This behavior is observed in Figs. 4(b) and 4(c), where the SW frequencies for $a = 50$ nm and 250 nm are compared. In addition, the amplitudes of the dynamic magnetization components are also equivalent as the curvature decreases (not shown). In principle, these similarities between planar and tubular systems are expected since, as a increases, curvature effects vanish, and the dynamic behavior of the tubular bilayer must be equivalent to the planar one. Nevertheless, the range of curvature where this matching occurs is not too extensive; it is just a few hundred nanometers, and it can be even lower if the thicknesses of the tubular layers decrease. This finding implies that magnetochiral properties are preserved in a cylindrical bilayer regardless of the radius of the internal tube. In isolated microtubes prepared from rolled-up ferromagnetic layers [90,91], for instance, the nonreciprocal features have not been observed since magnetochiral effects due to curvature are visible only for tube radius comparable with the exchange length of a few nanometers. In contrast, a tubular magnetic bilayer can manifest magnetochirality in the micrometer regime, not from curvature but the asymmetric interlayer dipolar coupling. Therefore, it can be concluded that the nonreciprocity observed in a tubular synthetic antiferromagnet stems mainly from the interlayer dipolar interaction described in Ref. [36] rather than the geometrical charges of the isolated nanotubes.

The previous results imply that analytical expressions can be used to estimate the magnonic dispersion and frequency shift of cylindrical synthetic antiferromagnets with thin layers ($d \leq \ell_{\mathrm{ex}}$). For instance, the frequency shift for two antiparallel coupled thin layers (see Eq. (8) of Ref. [36]) is

$$\Delta f_{\mathrm{AP}} = \frac{2\gamma}{\pi}\mu_0 M_s \sinh^2(kd/2)\frac{e^{-|k|(d+s)}}{kd}, \qquad (5)$$

where both ferromagnetic layers have a thickness d. Now, Δf_{AP} can be used to predict the frequency shift of CSAs with $a \gg \ell_{\mathrm{ex}}$. In Fig. 5, the formalism developed here is contrasted with the theory for planar bilayers [see Eq. (5)] evaluated at fixed inner radius $a = 40$ nm. For the cylindrical nanostructure, three cases are considered with exemplary shell thicknesses of $d_i = d_o = 2$, 4, and 8 nm. Similar layer thicknesses are used for the planar system.

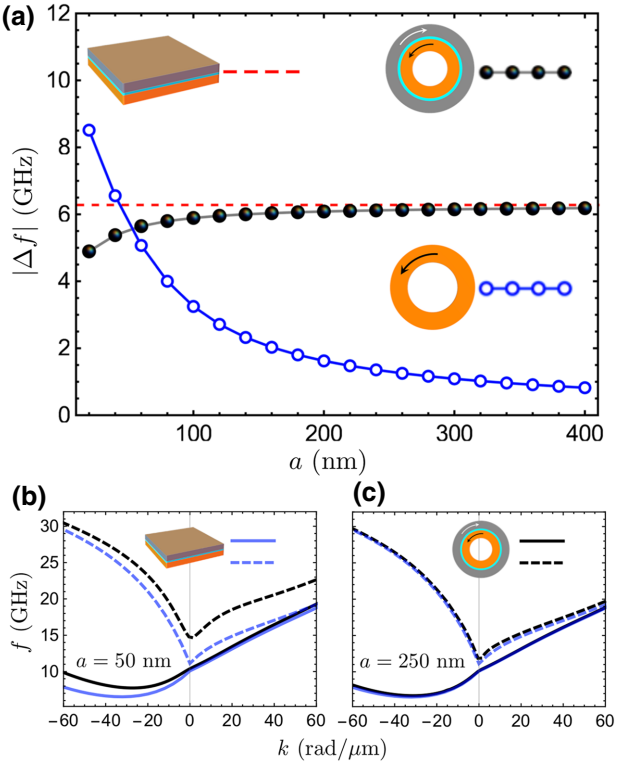

FIG. 4. (a) Spin-wave frequency shift induced by the dipolar interaction in different types of structures as a function of the internal radius a. Δf is evaluated at $|k| = 20$ rad/μm. The thickness of the isolated NT is $d = 30$ nm, while the thicknesses of the synthetic antiferromagnet layers are 15 nm. Open circles describe the case of one isolated nanotube, while the filled circles correspond to the cylindrical synthetic antiferromagnet. Dashed lines show the frequency shift of a planar synthetic antiferromagnet. SW dispersion for planar and cylindrical synthetic antiferromagnets evaluated at (b) $a = 50$ nm and (c) $a = 250$ nm. Darker (lighter) lines correspond to the modes of the tubular (planar) system.

An almost perfect agreement between both models is evidenced. As the thicknesses of the layers increase, the discrepancy between both theories increases, which is reasonable since the frequency shift Δf_{AP} is derived for thin films, where a homogeneous radial SW profile is assumed. Therefore, the dynamical properties of two oppositely magnetized nanotubes can be analytically handled with the expressions used for planar synthetic antiferromagnets, provided that the curvilinear shells of the system are thin and $a \gg \ell_{\mathrm{ex}}$. These results are beneficial for rapidly quantifying the nonreciprocal features of a tubular bilayer, allowing the influence of geometry on spin-wave dynamics to be visualized. Note that at small wave vectors, the frequency shift shown in Eq. (5) varies linearly with $\mathbf{k}$. Thus, according to Ref. [36], the contribution of the SW asymmetry induced by the dynamic dipolar interaction has the same characteristics as that induced by the interfacial Dzyaloshinskii-Moriya coupling. One can also note

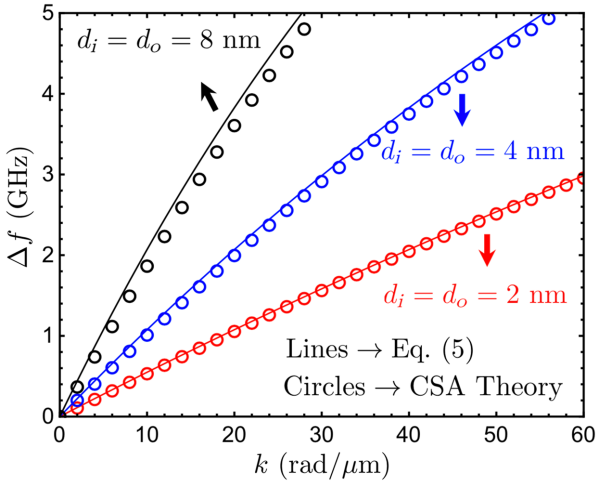

FIG. 5. Comparison between the frequency shift, obtained from the calculation of the curved bilayer structure, and the frequency shift estimated from the formula for flat bilayers given in Eq. (5). Three cases are considered, where the thicknesses of the cylindrical NTs [and layers, in the case of Eq. (5)] are 2, 4, and 6 nm. An inner radius $a = 40$ nm is used for the cylindrical synthetic antiferromagnet.

that Eq. (5) does not depend on the interlayer exchange constant in the small-curvature limit. Nonetheless, as the wave vector increases, the exchange coupling between layers influences the nonreciprocal properties of the spin waves. Indeed, as the exchange constant ξ increases, the SW asymmetry is reduced (not shown) because such an interlayer exchange interaction with nonchiral properties becomes relevant.

IV. SUMMARY

In conclusion, calculations demonstrate that the spin-wave spectrum of cylindrical synthetic antiferromagnets shows a chiral behavior. The nonreciprocal character of the waves is preserved as the nanotube radius increases, which is a notable advantage over the nonreciprocity of an isolated nanotube, where the spin-wave asymmetry vanishes as the curvature decreases. By analyzing the frequency dispersion as a function of curvature, it is found that the dynamic behavior of the tubular bilayer matches that of a planar synthetic antiferromagnetic when the radii are a few hundred nanometers. In the case of ultrathin layers, both planar and cylindrical synthetic antiferromagnets have similar magnetochiral properties. Therefore, analytical formulas can be used to estimate the frequency shift of the cylindrical synthetic antiferromagnet, which is very helpful in analyzing the influence of geometry on spin-wave dynamics. The proposed structure also shows a wide range of frequencies and wave vectors where unidirectional magnonic propagation is expected. These results are essential for envisioning future logic devices based on nonreciprocal wave propagation at the microscale and nanoscale.

ACKNOWLEDGMENTS

The authors acknowledge financial support from Fondecyt Grants No. 1210607 and No. 1201153, and Basal Program for Centers of Excellence, Grant No. AFB180001 CEDENNA, CONICYT.

[1] Sebastian Neusser and Dirk Grundler, Magnonics: Spin waves on the nanoscale, Adv. Mater. **21**, 2927 (2009).
[2] V. V. Kruglyak, S. O. Demokritov, and D. Grundler, Magnonics, J. Phys. D: Appl. Phys. **43**, 264001 (2010).
[3] B. Lenk, H. Ulrichs, F. Garbs, and M. Münzenberg, The building blocks of magnonics, Phys. Rep. **507**, 107 (2011).
[4] A. V. Chumak, V. I. Vasyuchka, A. A. Serga, and B. Hillebrands, Magnon spintronics, Nat. Phys. **11**, 453 (2015).
[5] Dirk Grundler, Nanomagnonics around the corner, Nat. Nanotechnol. **11**, 407 (2016).
[6] Gianluca Gubbiotti, (Ed.), *Three-dimensional magnonics: layered, micro-and nanostructures*, (Jenny Stanford Publishing, 2019).
[7] Anjan Barman, *et al.*, The 2021 magnonics roadmap, J. Phys. Condens. Matter **33**, 413001 (2021).
[8] Haiming Yu, G. Duerr, R. Huber, M. Bahr, T. Schwarze, F. Brandl, and D. Grundler, Omnidirectional spin-wave nanograting coupler, Nat. Commun. **4**, 2702 (2013).
[9] Haiming Yu, O. d'Allivy Kelly, V. Cros, R. Bernard, P. Bortolotti, A. Anane, F. Brandl, F. Heimbach, and D. Grundler, Approaching soft x-ray wavelengths in nanomagnet-based microwave technology, Nat. Commun. **7**, 11255 (2016).
[10] Chuanpu Liu, Jilei Chen, Tao Liu, Florian Heimbach, Haiming Yu, Yang Xiao, Junfeng Hu, Mengchao Liu, Houchen Chang, Tobias Stueckler, Sa Tu, Youguang Zhang, Yan Zhang, Peng Gao, Zhimin Liao, Dapeng Yu, Ke Xia, Na Lei, Weisheng Zhao, and Mingzhong Wu, Long-distance propagation of short-wavelength spin waves, Nat. Commun. **9**, 738 (2018).
[11] Ping Che, Korbinian Baumgaertl, Anna Kúkol'ová, Carsten Dubs, and Dirk Grundler, Efficient wavelength conversion of exchange magnons below 100 nm by magnetic coplanar waveguides, Nat. Commun. **11**, 1445 (2020).
[12] Alexander G. Gurevich and Gennadii A. Melkov, *Magnetization Oscillations and Waves* (CRC Press, Inc, 1996).
[13] M. Krawczyk and D. Grundler, Review and prospects of magnonic crystals and devices with reprogrammable band structure, J. Phys. Condens. Matter. **26**, 123202 (2014).
[14] Markus Garst, Johannes Waizner, and Dirk Grundler, Collective spin excitations of helices and magnetic skyrmions: Review and perspectives of magnonics in non-centrosymmetric magnets, J. Phys. D: Appl. Phys. **50**, 293002 (2017).
[15] Haiming Yu, Jiang Xiao, and Helmut Schultheiss, Magnetic texture based magnonics, Phys. Rep. **905**, 1 (2021).
[16] R. E. Camley, Nonreciprocal surface waves, Surf. Sci. Rep. **7**, 103 (1987).

[17] Jin Lan, Weichao Yu, Ruqian Wu, and Jiang Xiao, Spin-Wave Diode, Phys. Rev. X **5**, 041049 (2015).
[18] Negar Reiskarimian and Harish Krishnaswamy, Magnetic-free non-reciprocity based on staggered commutation, Nat. Commun. **7**, 11217 (2016).
[19] Dimitrios L. Sounas and Andrea Alù, Non-reciprocal photonics based on time modulation, Nat. Photonics **11**, 774 (2017).
[20] Jilei Chen, Junfeng Hu, and Haiming Yu, Chiral magnonics: Reprogrammable nanoscale spin wave networks based on chiral domain walls, iScience **23**, 101153 (2020).
[21] K. G. Fripp, A. V. Shytov, and V. V. Kruglyak, Spin-wave control using dark modes in chiral magnonic resonators, Phys. Rev. B **104**, 054437 (2021).
[22] R. A. Gallardo, P. Alvarado-Seguel, T. Schneider, C. Gonzalez-Fuentes, A. Roldán-Molina, K. Lenz, J. Lindner, and P. Landeros, Spin-wave non-reciprocity in magnetization-graded ferromagnetic films, New J. Phys. **21**, 033026 (2019).
[23] Jorge A. Otálora, Ming Yan, Helmut Schultheiss, Riccardo Hertel, and Attila Kákay, Curvature-Induced Asymmetric Spin-Wave Dispersion, Phys. Rev. Lett. **117**, 227203 (2016).
[24] Jorge A. Otálora, Ming Yan, Helmut Schultheiss, Riccardo Hertel, and Attila Kákay, Asymmetric spin-wave dispersion in ferromagnetic nanotubes induced by surface curvature, Phys. Rev. B **95**, 184415 (2017).
[25] Denis D. Sheka, Oleksandr V. Pylypovskyi, Pedro Landeros, Yuri Gaididei, Attila Kákay, and Denys Makarov, Nonlocal chiral symmetry breaking in curvilinear magnetic shells, Commun. Phys. **3**, 128 (2020).
[26] L. Körber, G. Quasebarth, A. Otto, and A. Kákay, Finite-element dynamic-matrix approach for spin-wave dispersions in magnonic waveguides with arbitrary cross section, AIP Adv. **11**, 095006 (2021).
[27] L. Körber and A. Kákay, Numerical reverse engineering of general spin-wave dispersions: Bridge between numerics and analytics using a dynamic-matrix approach, Phys. Rev. B **104**, 174414 (2021).
[28] R. A. Gallardo, P. Alvarado-Seguel, and P. Landeros, High spin-wave asymmetry and emergence of radial standing modes in thick ferromagnetic nanotubes, Phys. Rev. B **105**, 104435 (2022).
[29] Lukas Körber, Roman Verba, Jorge A. Otálora, Volodymyr Kravchuk, Jürgen Lindner, Jürgen Fassbender, and Attila Kákay, Curvilinear spin-wave dynamics beyond the thin-shell approximation: Magnetic nanotubes as a case study, Phys. Rev. B **106**, 014405 (2022).
[30] Roman Verba, Vasil Tiberkevich, Elena Bankowski, Thomas Meitzler, Gennadiy Melkov, and Andrei Slavin, Conditions for the spin wave nonreciprocity in an array of dipolarly coupled magnetic nanopillars, Appl. Phys. Lett. **103**, 082407 (2013).
[31] K. Mika and P. Grünberg, Dipolar spin-wave modes of a ferromagnetic multilayer with alternating directions of magnetization, Phys. Rev. B **31**, 4465 (1985).
[32] P. Grünberg, Some ways to modify the spin-wave mode spectra of magnetic multilayers (invited), J. Appl. Phys. **57**, 3673 (1985).
[33] P. Grünberg, R. Schreiber, Y. Pang, M. B. Brodsky, and H. Sowers, Layered Magnetic Structures: Evidence for Antiferromagnetic Coupling of Fe Layers Across Cr Interlayers, Phys. Rev. Lett. **57**, 2442 (1986).
[34] P. X. Zhang and W. Zinn, Spin-wave modes in antiparallel magnetized ferromagnetic double layers, Phys. Rev. B **35**, 5219 (1987).
[35] G. Binasch, P. Grünberg, F. Saurenbach, and W. Zinn, Enhanced magnetoresistance in layered magnetic structures with antiferromagnetic interlayer exchange, Phys. Rev. B **39**, 4828 (1989).
[36] R. A. Gallardo, T. Schneider, A. K. Chaurasiya, A. Oelschlägel, S. S. P. K. Arekapudi, A. Roldán-Molina, R. Hübner, K. Lenz, A. Barman, J. Fassbender, J. Lindner, O. Hellwig, and P. Landeros, Reconfigurable Spin-Wave Nonreciprocity Induced by Dipolar Interaction in a Coupled Ferromagnetic Bilayer, Phys. Rev. Appl. **12**, 034012 (2019).
[37] Volker Sluka, Tobias Schneider, Rodolfo A. Gallardo, Attila Kákay, Markus Weigand, Tobias Warnatz, Roland Mattheis, Alejandro Roldán-Molina, Pedro Landeros, Vasil Tiberkevich, Andrei Slavin, Gisela Schütz, Artur Erbe, Alina Deac, Jürgen Lindner, Jörg Raabe, Jürgen Fassbender, and Sebastian Wintz, Emission and propagation of 1D and 2D spin waves with nanoscale wavelengths in anisotropic spin textures, Nat. Nanotechnol. **14**, 328 (2019).
[38] Mio Ishibashi, Yoichi Shiota, Tian Li, Shinsaku Funada, Takahiro Moriyama, and Teruo Ono, Switchable giant nonreciprocal frequency shift of propagating spin waves in synthetic antiferromagnets, Sci. Adv. **6**, eaaz6931 (2020).
[39] Edoardo Albisetti, Silvia Tacchi, Raffaele Silvani, Giuseppe Scaramuzzi, Simone Finizio, Sebastian Wintz, Christian Rinaldi, Matteo Cantoni, Jörg Raabe, Giovanni Carlotti, Riccardo Bertacco, Elisa Riedo, and Daniela Petti, Optically inspired nanomagnonics with nonreciprocal spin waves in synthetic antiferromagnets, Adv. Mater. **32**, 1906439 (2020).
[40] R. A. Gallardo, P. Alvarado-Seguel, A. Kákay, J. Lindner, and P. Landeros, Spin-wave focusing induced by dipole-dipole interaction in synthetic antiferromagnets, Phys. Rev. B **104**, 174417 (2021).
[41] Matías Grassi, Moritz Geilen, Damien Louis, Morteza Mohseni, Thomas Brächer, Michel Hehn, Daniel Stoeffler, Matthieu Bailleul, Philipp Pirro, and Yves Henry, Slow-Wave-Based Nanomagnonic Diode, Phys. Rev. Appl. **14**, 024047 (2020).
[42] D. Cortés-Ortuño and P. Landeros, Influence of the Dzyaloshinskii–Moriya interaction on the spin-wave spectra of thin films, J. Phys: Cond. Matt. **25**, 156001 (2013).
[43] Jung-Hwan Moon, Soo-Man Seo, Kyung-Jin Lee, Kyoung-Whan Kim, Jisu Ryu, Hyun-Woo Lee, R. D. McMichael, and M. D. Stiles, Spin-wave propagation in the presence of interfacial Dzyaloshinskii-Moriya interaction, Phys. Rev. B **88**, 184404 (2013).
[44] Kai Di, Vanessa Li Zhang, Hock Siah Lim, Ser Choon Ng, Meng Hau Kuok, Jiawei Yu, Jungbum Yoon, Xuepeng Qiu, and Hyunsoo Yang, Direct Observation of the Dzyaloshinskii-Moriya Interaction in a Pt/Co/Ni Film, Phys. Rev. Lett. **114**, 047201 (2015).

[45] Jaehun Cho, Nam-Hui Kim, Sukmock Lee, June-Seo Kim, Reinoud Lavrijsen, Aurelie Solignac, Yuxiang Yin, Dong-Soo Han, Niels J. J. van Hoof, Henk J. M. Swagten, Bert Koopmans, and Chun-Yeol You, Thickness dependence of the interfacial Dzyaloshinskii–Moriya interaction in inversion symmetry broken systems, Nat. Commun. **6**, 7635 (2015).

[46] Hans T. Nembach, Justin M. Shaw, Mathias Weiler, Emilie Jue, and Thomas J. Silva, Linear relation between Heisenberg exchange and interfacial Dzyaloshinskii-Moriya interaction in metal films, Nat. Phys. **11**, 825 (2015).

[47] Mohamed Belmeguenai, Jean-Paul Adam, Yves Roussigné, Sylvain Eimer, Thibaut Devolder, Joo-Von Kim, Salim Mourad Cherif, Andrey Stashkevich, and André Thiaville, Interfacial Dzyaloshinskii-Moriya interaction in perpendicularly magnetized Pt/Co/AlO_x ultrathin films measured by Brillouin light spectroscopy, Phys. Rev. B **91**, 180405(R) (2015).

[48] Avinash Kumar Chaurasiya, Chandrima Banerjee, Santanu Pan, Sourav Sahoo, Samiran Choudhury, Jaivardhan Sinha, and Anjan Barman, Direct observation of interfacial Dzyaloshinskii-Moriya interaction from asymmetric spin-wave propagation in W/CoFeB/SiO_2 heterostructures down to sub-nanometer CoFeB thickness, Sci. Rep. **6**, 32592 (2016).

[49] S. Tacchi, R. E. Troncoso, M. Ahlberg, G. Gubbiotti, M. Madami, J. Åkerman, and P. Landeros, Interfacial Dzyaloshinskii-Moriya Interaction in Pt/CoFeB Films: Effect of the Heavy-Metal Thickness, Phys. Rev. Lett. **118**, 147201 (2017).

[50] Avinash Kumar Chaurasiya, Samiran Choudhury, Jaivardhan Sinha, and Anjan Barman, Dependence of Interfacial Dzyaloshinskii-Moriya Interaction on Layer Thicknesses in Ta/Co-Fe-B/TaO_x Heterostructures from Brillouin Light Scattering, Phys. Rev. Appl. **9**, 014008 (2018).

[51] R. A. Gallardo, D. Cortés-Ortuño, R. E. Troncoso, and P. Landeros, Three-dimensional magnonics: layered, micro- and nanostructures, (Jenny Stanford Publishing, Berlin, Heidelberg, 2019), p. 121.

[52] Y. Iguchi, S. Uemura, K. Ueno, and Y. Onose, Nonreciprocal magnon propagation in a noncentrosymmetric ferromagnet $LiFe_5O_8$, Phys. Rev. B **92**, 184419 (2015).

[53] S. Seki, Y. Okamura, K. Kondou, K. Shibata, M. Kubota, R. Takagi, F. Kagawa, M. Kawasaki, G. Tatara, Y. Otani, and Y. Tokura, Magnetochiral nonreciprocity of volume spin wave propagation in chiral-lattice ferromagnets, Phys. Rev. B **93**, 235131 (2016).

[54] T. Weber, J. Waizner, G. S. Tucker, L. Beddrich, M. Skoulatos, R. Georgii, A. Bauer, C. Pfleiderer, M. Garst, and P. Böni, Non-reciprocal magnons in non-centrosymmetric MnSi, AIP Adv. **8**, 101328 (2018).

[55] Taku J. Sato and Kittiwit Matan, Nonreciprocal magnons in noncentrosymmetric magnets, J. Phys. Soc. Jpn. **88**, 081007 (2019).

[56] Martin Lonsky and Axel Hoffmann, Dynamic excitations of chiral magnetic textures, APL Mater. **8**, 100903 (2020).

[57] K. Di, S. X. Feng, S. N. Piramanayagam, V. L. Zhang, H. S. Lim, S. C. Ng, and M. H. Kuok, Enhancement of spin-wave nonreciprocity in magnonic crystals via synthetic antiferromagnetic coupling, Sci. Rep. **5**, 10153 (2015).

[58] P. Alvarado-Seguel and R. A. Gallardo, Band structure of a one-dimensional bilayer magnonic crystal, Phys. Rev. B **100**, 144415 (2019).

[59] R. A. Gallardo, D. Cortés-Ortuño, T. Schneider, A. Roldán-Molina, Fusheng Ma, R. E. Troncoso, K. Lenz, H. Fangohr, J. Lindner, and P. Landeros, Flat Bands, Indirect Gaps, and Unconventional Spin-Wave Behavior Induced by a Periodic Dzyaloshinskii-Moriya Interaction, Phys. Rev. Lett. **122**, 067204 (2019).

[60] Zhongqiang Hu, Liang Fu, and Luqiao Liu, Tunable Magnonic Chern Bands and Chiral Spin Currents in Magnetic Multilayers, Phys. Rev. Lett. **128**, 217201 (2022).

[61] Jilei Chen, Haiming Yu, and Gianluca Gubbiotti, Unidirectional spin-wave propagation and devices, J. Phys. D: Appl. Phys. **55**, 123001 (2021).

[62] Kin L. Wong, Lei Bi, Mingqiang Bao, Qiye Wen, Jean Pierre Chatelon, Yen-Ting Lin, C. A. Ross, Huaiwu Zhang, and Kang L. Wang, Unidirectional propagation of magnetostatic surface spin waves at a magnetic film surface, Appl. Phys. Lett. **105**, 232403 (2014).

[63] R. W. Damon and J. R. Eshbach, Magnetostatic modes of a ferromagnet slab, J. Phys. Chem. Solids **19**, 308 (1961).

[64] Fusheng Ma and Yan Zhou, Interfacial Dzialoshinskii–Moriya interaction induced nonreciprocity of spin waves in magnonic waveguides, RSC Adv. **4**, 46454 (2014).

[65] T. Brächer, O. Boulle, G. Gaudin, and P. Pirro, Creation of unidirectional spin-wave emitters by utilizing interfacial Dzyaloshinskii-Moriya interaction, Phys. Rev. B **95**, 064429 (2017).

[66] Y. Henry, D. Stoeffler, J.-V. Kim, and M. Bailleul, Unidirectional spin-wave channeling along magnetic domain walls of Bloch type, Phys. Rev. B **100**, 024416 (2019).

[67] Jilei Chen, Tao Yu, Chuanpu Liu, Tao Liu, Marco Madami, Ka Shen, Jianyu Zhang, Sa Tu, Md Shah Alam, Ke Xia, Mingzhong Wu, Gianluca Gubbiotti, Yaroslav M. Blanter, Gerrit E. W. Bauer, and Haiming Yu, Excitation of unidirectional exchange spin waves by a nanoscale magnetic grating, Phys. Rev. B **100**, 104427 (2019).

[68] Krzysztof Szulc, Piotr Graczyk, Michał Mruczkiewicz, Gianluca Gubbiotti, and Maciej Krawczyk, Spin-Wave Diode and Circulator Based on Unidirectional Coupling, Phys. Rev. Appl. **14**, 034063 (2020).

[69] R. Hertel, Computational micromagnetism of magnetization processes in nickel nanowires, J. Magn. Magn. Mater. **249**, 251 (2002).

[70] P. Landeros, S. Allende, J. Escrig, E. Salcedo, D. Altbir, and E. E. Vogel, Reversal modes in magnetic nanotubes, Appl. Phys. Lett. **90**, 102501 (2007).

[71] P. Landeros, O. J. Suarez, A. Cuchillo, and P. Vargas, Equilibrium states and vortex domain wall nucleation in ferromagnetic nanotubes, Phys. Rev. B **79**, 024404 (2009).

[72] D. Rüffer, R. Huber, P. Berberich, S. Albert, E. Russo-Averchi, M. Heiss, J. Arbiol, A. Fontcuberta i Morral, and D. Grundler, Magnetic states of an individual Ni nanotube probed by anisotropic magnetoresistance, Nanoscale **4**, 4989 (2012).

[73] Daniel Rüffer, Marlou Slot, Rupert Huber, Thomas Schwarze, Florian Heimbach, Gözde Tütüncüoglu, Federico Matteini, Eleonora Russo-Averchi, András Kovács,

Rafal Dunin-Borkowski, Reza R. Zamani, Joan R. Morante, Jordi Arbiol, Anna Fontcuberta i Morral, and Dirk Grundler, Anisotropic magnetoresistance of individual CoFeB and Ni nanotubes with values of up to 1.4% at room temperature, APL Mater. **2**, 076112 (2014).

[74] R. Streubel, F. Kronast, P. Fischer, D. Parkinson, O. G. Schmidt, and D. Makarov, Retrieving spin textures on curved magnetic thin films with full-field soft x-ray microscopies, Nat. Commun. **6**, 7612 (2015).

[75] Michal Staño and Olivier Fruchart, Magnetic nanowires and nanotubes, Handbook Magn. Mater. **27**, 155 (2018).

[76] P. Landeros and Á. S. Núñez, Domain wall motion on magnetic nanotubes, J. Appl. Phys. **108**, 033917 (2010).

[77] J. A. Otálora, J. A. López-López, P. Vargas, and P. Landeros, Chirality switching and propagation control of a vortex domain wall in ferromagnetic nanotubes, Appl. Phys. Lett. **100**, 072407 (2012).

[78] J. A. Otálora, J. A. López-López, P. Landeros, P. Vargas, and A. S. Núñez, Breaking of chiral symmetry in vortex domain wall propagation in ferromagnetic nanotubes, J. Magn. Magn. Mater. **341**, 86 (2013).

[79] Ming Yan, Christian Andreas, Attila Kákay, Felipe García-Sánchez, and Riccardo Hertel, Chiral symmetry breaking and pair-creation mediated walker breakdown in magnetic nanotubes, Appl. Phys. Lett. **100**, 252401 (2012).

[80] R. Hertel, Curvature-induced magnetochirality, Spin **03**, 1340009 (2013).

[81] Robert Streubel, Peter Fischer, Florian Kronast, Volodymyr P. Kravchuk, Denis D Sheka, Yuri Gaididei, Oliver G. Schmidt, and Denys Makarov, Magnetism in curved geometries, J. Phys. D: Appl. Phys. **49**, 363001 (2016).

[82] Denys Makarov, Oleksii M. Volkov, Attila Kákay, Oleksandr V. Pylypovskyi, Barbora Budinská, and Oleksandr V. Dobrovolskiy, New dimension in magnetism and superconductivity: 3D and curvilinear nanoarchitectures, Adv. Mater. **34**, 2101758 (2021).

[83] Denis D. Sheka, A perspective on curvilinear magnetism, Appl. Phys. Lett. **118**, 230502 (2021).

[84] Lukas Körber, Michael Zimmermann, Sebastian Wintz, Simone Finizio, Matthias Kronseder, Dominique Bougeard, Florian Dirnberger, Markus Weigand, Jörg Raabe, Jorge A. Otálora, Helmut Schultheiss, Elisabeth Josten, Jürgen Lindner, István Kézsmárki, Christian H. Back, and Attila Kákay, Symmetry and curvature effects on spin waves in vortex-state hexagonal nanotubes, Phys. Rev. B **104**, 184429 (2021).

[85] M. Krawczyk and H. Puszkarski, Plane-wave theory of three-dimensional magnonic crystals, Phys. Rev. B **77**, 054437 (2008).

[86] Y. Henry, O. Gladii, and M. Bailleul, Propagating spin-wave normal modes: A dynamic matrix approach using plane-wave demagnetizating tensors, (2016), ArXiv:1611.06153.

[87] J. Brandão, S. Azzawi, A. T. Hindmarch, and D. Atkinson, Understanding the role of damping and Dzyaloshinskii-Moriya interaction on dynamic domain wall behaviour in platinum-ferromagnet nanowires, Sci. Rep. **7**, 4569 (2017).

[88] As a reference, for $a = 78$ nm and $d_i = d_o = 4$ nm, such a ξ value is equivalent to $J = -1$ mJ/m^2, which is a standard value of the interlayer exchange constant of planar bilayer structures.

[89] A value of $J = -0.2$ mJ/m^2 has been used, which is taken from $J = \xi/(2\pi a)$ by considering $a = 400$ nm. For larger values of a, there is no change in the frequency shift of a planar synthetic antiferromagnet.

[90] Felix Balhorn, Simon Jeni, Wolfgang Hansen, Detlef Heitmann, and Stefan Mendach, Axial and azimuthal spin-wave eigenmodes in rolled-up permalloy stripes, Appl. Phys. Lett. **100**, 222402 (2012).

[91] Felix Balhorn, Cornelius Bausch, Simon Jeni, Wolfgang Hansen, Detlef Heitmann, and Stefan Mendach, Azimuthal spin-wave modes in rolled-up permalloy microtubes: Tuneable mode frequency, mode patterns, and mode splitting, Phys. Rev. B **88**, 054402 (2013).